# A Multiresolution MoM Analysis of Multiport Structures Using Matched Terminations

Renaud Loison, Raphaël Gillard, Jacques Citerne, *Member, IEEE*, Gerard Piton, and H. Legay

***Abstract*—This paper presents the modeling of microstrip structures involving matched terminations with a one-dimensional multiresolution method of moment (MRMoM). Semiorthogonal spline wavelets are used as basis and testing functions. For large structures, the MRMoM generates a sparse linear system, which permits a significant reduction of the central processing unit time and of the memory storage. The modeling of matched terminations also enables a full characterization of multiport microstrip structures. Theoretical results involving microstrip dipoles are presented and compared with experiments.**

***Index Terms*—Method of moments, wavelets.**

## I. Introduction

THE method of moments (MoM) is a well-known technique to numerically solve the electric-field integral equation (EFIE) encountered in electromagnetic problems [1]. Unfortunately, this technique leads to a large and dense matrix, which often becomes computationally intractable when fine discretizations or large structures are involved.

To overcome these difficulties, the use of wavelets bases is often proposed. In practice, two main solutions are offered to use them. On one hand, the impedance matrix computed in the conventional MoM can be compressed as an image with the help of the discrete wavelet transform (DWT) [2]–[5]. On the other hand, wavelets can be directly used as basis and testing functions in the MoM [6]–[8]. In both cases, the technique leads to a sparse impedance matrix, which can be efficiently solved by a sparse solver. This paper deals with the second approach.

As in [7] and [8], semiorthogonal (SO) spline wavelets of order 2 are chosen as basis functions as well as testing ones. These functions are known as Chui wavelets [10] and are defined on a bounded interval. It is shown, as in [7] and [8], that the use of this basis leads to a sparse system. In this paper, precise rules are given to efficiently calculate and store the matrix. A novel multiscale approach of the calculation allows direct computation of the sparse system and, hence, avoids the storage of a dense matrix. It is shown that the sparsity increases with the size of the linear system. Since large structures are usually multiport structures, it is important for the multiresolution analysis to be able to take matched terminations into account. To this end, a new formulation of the matched load model, in the wavelet basis, is proposed. This model, associated to the calculation rules, permits the analysis of large linear arrays of microstrip electromagnetically coupled (EMC) dipoles. The multiresolution method of moments (MRMoM) analysis of these examples demonstrates the efficiency of the proposed approach compared to the conventional MoM technique.

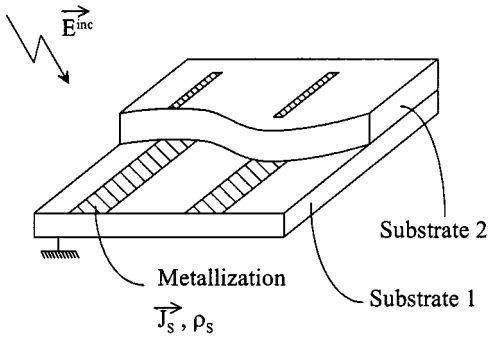


Fig. 1. Typical 1-D microstrip structure.

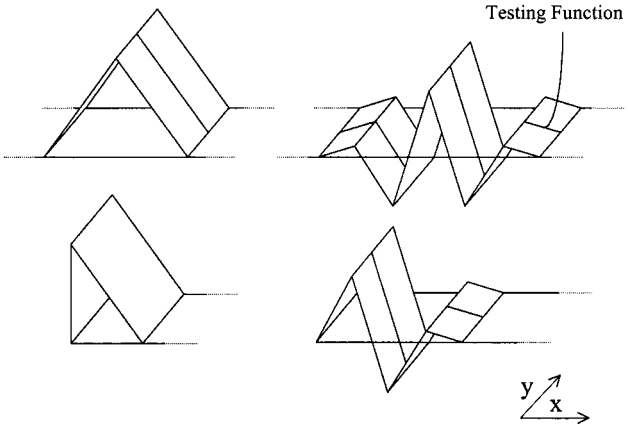


Fig. 2. Basis and testing functions.

First, the application of wavelets in the MoM is presented. Second, the formulation of the matched load model is described. Then, in order to optimize the CPU time and memory storage, different steps of the implementation are specified. The capabilities of the proposed technique are then illustrated with the simulation of linear arrays of microstrip dipoles. To conclude, a comparison with the DWT application is made and the limitations and advantages of solving integral equations with Chui wavelet expansion are discussed.

## II. MoM with Chui Wavelets

### A. MoM Formulation

A typical one-dimensional (1-D) microstrip structure is shown in Fig. 1. The EFIE can be written as the following

Manuscript received July 22, 1999. This work was supported by the Centre National des Etudes Spatiales and by Alcatel Space Industries.

R. Loison, R. Gillard, and J. Citerne are with Laboratory for Telecommunication Components and Systems, National Institute of Applied Sciences, 35043 Rennes, France (e-mail: Renaud.Loison@insa-rennes.fr)

G. Piton is with the Centre National d'Etudes Spatiales, Toulouse 31401, France

H. Legay is with Alcatel Space Industries, Toulouse 31100, France.

Publisher Item Identifier S 0018-9480(01)00032-1.

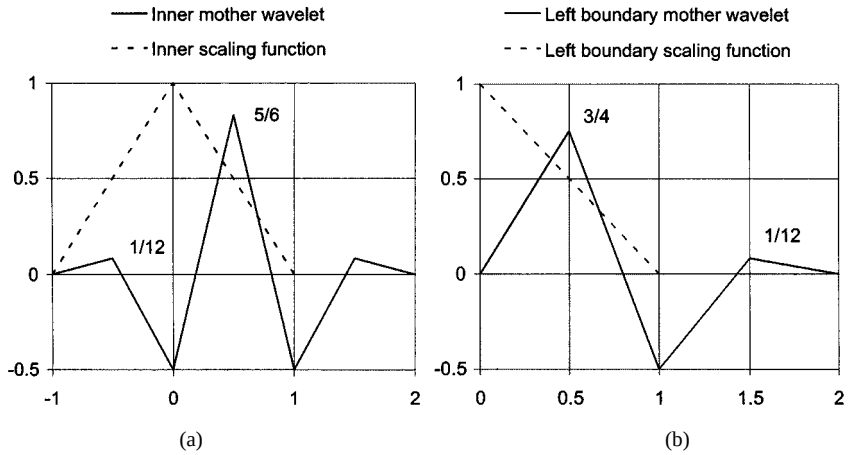


Fig. 3. Chui basis.

mixed-potential integral equation (MPIE) [1]:

$$\vec{e}_n \times \vec{E}^{\text{inc}}(\vec{r}) = \vec{e}_n \times \left[ \iint_{S'} \left[ j\omega \overline{\overline{G_A}}(\vec{r}/\vec{r}\,') \vec{J}_S(\vec{r}\,') + \vec{\nabla} G_V(\vec{r}/\vec{r}\,') \rho_S(\vec{r}\,') \right] dS' \right] \quad (1)$$

where $\rho_s$ is the charge density and is related to the surface current $\vec{J}_S$ by the continuity equation. $\overline{\overline{G_A}}$ and $G_V$ are the multilayered dielectric dyadic and scalar Green's functions [11] and $\vec{e}_n$ is the unit vector perpendicular to the surface of the conductor. The aim of the MoM is to determine the surface current flowing on the metallizations. This surface current is induced by an excitation that can be an incident electric field ($\vec{E}^{\text{inc}}$) or a current generator. Since only electrically narrow structures are considered here, the analysis is restricted to the longitudinal current. This limits the applications of the presented technique to the analysis of thin microstrip lines or dipoles whose width is small compared to the wavelength.

The surface current is expanded on a set of basis functions, and (1) is weighted using a set of testing functions. This yields the linear system

$$[Z][I] = [V]. \quad (2)$$

Here, $[Z]$ is the impedance matrix, while $[I]$ and $[V]$ are the vectors of the unknown current coefficients and the tested incident electric field, respectively. This linear system must be solved in order to calculate the unknown coefficients $[I]$. The elements of the impedance matrix are obtained from

$$Z_{ij} = j\omega \iint_{S_i} \iint_{S'_j} \vec{f}_{t,i}(\vec{r}) \overline{\overline{G_A}}(\vec{r}/\vec{r}\,') \vec{f}_{b,j}(\vec{r}\,')\, dS_i\, dS'_j + \frac{j}{\omega} \iint_{S_i} \iint_{S'_j} \vec{f}_{t,i}(\vec{r}) \vec{\nabla} G_V(\vec{r}/\vec{r}\,') \vec{\nabla}' \vec{f}_{b,j}(\vec{r}\,')\, dS_i\, dS'_j \quad (3)$$

where $\vec{f}_{t,i}(\vec{r})$ and $\vec{f}_{b,j}(\vec{r}\,')$ are the testing and expansion functions, respectively, and $S_i$ and $S'_j$ are the supports of these functions.

### B. Chui Wavelet Basis

Efficiency and accuracy of the computation can be improved by the choice of good bases. A function $\psi(u)$ is said to have a vanishing moment of order $n$ if

$$\int \psi(u) u^{n-1} = 0. \quad (4)$$

If Green's functions are smooth enough to be approximated by a polynomial expression of order $N$, and if the basis or the testing function has $N$ vanishing moments of order $(1, \ldots, N)$, then (3) clearly shows that the associated matrix element vanishes or becomes very small. Since wavelets have vanishing moments properties, they are suitable candidates as basis and testing functions [6]. It can be noticed that if both basis and testing functions have vanishing moments, the cancellation effect will be more important, which suggests a Galerkin scheme.

In this paper, basis functions are two-dimensional ones (Fig. 2). In the longitudinal direction, Chui wavelet basis of order 2 is chosen, while in the transverse direction, classical pulse functions are applied. On the other hand, testing functions are reduced to 1-D functions, which are the Chui functions in the longitudinal direction and Dirac functions in the transverse one. This choice keeps the advantages of the Galerkin scheme while suppressing one integration in (3).

The Chui system is SO and is generated by two different functions. The scaling function is the well-known rooftop, while the mother wavelet is a piecewise linear function (Fig. 3). This wavelet has a finite support, is symmetric, and has a simple analytical expression. Since Chui basis is defined on a bounded interval, special functions are introduced at the boundaries. As in [8], the special wavelets are chosen with vanishing values at the boundaries. The inner wavelet has two vanishing moments, while the special boundary wavelet has only one vanishing moment of order 2.

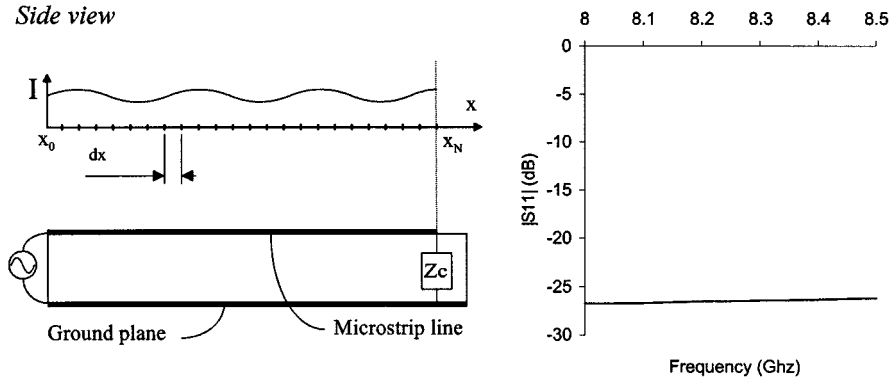


(a) (b)

Fig. 4. Matched termination (propagation in the $x$-direction) and return loss versus frequency.

The functions of the Chui basis are the dilated and translated versions of these mother wavelets and scaling functions as follows:

$$\phi_{s,k}(u) = \phi(2^s u - k) \quad \psi_{s,k}(u) = \psi(2^s u - k) \tag{5}$$

where $\phi(u)$ is the scaling function, $\psi(u)$ is the mother wavelet, $k$ is the translation factor, and $s$ is the resolution level. The multiresolution expansion of the surface current flowing on a 1-D microstrip metallization oriented along the $x$ axis then takes the following form:

$$\vec{J}_S(\vec{r}) = \vec{e}_x \left[ \sum_{k=0}^{2^{s_0}} I^{\Phi}_{s_0,k} \Phi_{s_0,k}(\vec{r}) + \sum_{s=s_0}^{s_u} \sum_{k=0}^{2^s-1} I^{\Psi}_{s,k} \Psi_{s,k}(\vec{r}) \right] \tag{6}$$

where $\vec{e}_x$ is the unit vector of the $x$ axis, $I^{\Phi}_{s_0,k}$ and $I^{\Psi}_{s,k}$ are the unknown coefficients associated with the scaling function and the wavelets, and $s_0$ and $s_u$ indicate the coarsest and finest resolution levels, respectively. In practice, the multilevel decomposition starts at the coarsest possible level (the smallest $s_0$ as possible). By this means, the number of scaling functions that produce the dense part of the impedance matrix is reduced. For the Chui basis, the lowest resolution level is $s_0 = 2$. Under this value, the associated wavelet $\psi_{s_0}$ has a support larger than the interval, which is not physical. In (6), because of the two-dimensional nature of the basis functions, these wavelets are noted with capital letters. In the expansion, $\Phi_{s_0,0}(\vec{r})$ and $\Phi_{s_0,2^{s_0}}(\vec{r})$ are left- and right-hand-side half-rooftops, while $\Psi_{s,0}(\vec{r})$ and $\Psi_{s,2^s-1}(\vec{r})$ are left- and right-hand-side boundary wavelets. A half-rooftop is used only when the surface current does not vanish at the corresponding metallization extremity, or in other words, when an excitation or a matched load is placed at this extremity. There are no testing functions associated with the two half-rooftops. It is possible to use these two corresponding equations of the linear system to set the boundary currents to the desired value.

As is shown in [7], Chui basis of order 2 is a suitable choice for the MRMoM. The Chui system combines the advantages of both rooftops and wavelets.

## III. Matched Load

In the MRMoM, the current density is expanded on a wavelet basis. In order to simulate a matched termination, we have to give a new formulation of the model presented in [9]. If we consider Fig. 4(a), the formulation of the matched load model is

$$J(x_n) = \left(\frac{1}{N_{\text{ref}}}\right)\left(\sum_{p=n-1}^{n-N_{\text{ref}}} J(x_p).\exp(-j\beta(n-p)\,dx)\right)$$

with

$$n = N,\, N-1,\, \ldots,\, N - N_{\text{cond}} - 1. \tag{7}$$

In fact, this equation can be seen as an absorbing condition. The current density at a plane of the line ($x_n$) is forced to be equal to the average of the current densities at $N_{\text{ref}}$ reference planes ($x_p$) with the corresponding phase shifts. This condition is applied at $N_{\text{cond}}$ planes at the end of the line and generates $N_{\text{cond}}$ equations. The main difference with [9] is that because of the wavelet expansion (6), each current density taken at a reference plane is not simply associated to a single unknown coefficient. Since the supports of wavelets and scaling functions overlap at an arbitrary plane of the microstrip line, the current density is related to several unknown coefficients, as can be seen from (6).

The $N_{\text{cond}}$ equations (7) are added in the linear system where they replace the projections on the boundary testing functions. In the case of a matched load placed at the right-hand side of the line, these functions are

$$\Phi_{s_0,2^{s_0}},\, \Psi_{S,(2^S-1)}, \qquad \text{with} \quad S = s_u,\, \ldots,\, (s_u - N_{\text{cond}} + 2). \tag{8}$$

Experimentally, good results are obtained with $N_{\text{cond}} = 3$ and $N_{\text{ref}} = 7$. Fig. 4(b) shows the return loss for a matched microstrip line calculated with these parameters.

## IV. Numerical Optimization

The principal advantage of using wavelets in the MoM is the sparsity of the calculated impedance matrices. To fully benefit from the wavelet scheme in terms of CPU time and memory storage, it is first essential to predict in advance which coefficients of the matrix can be omitted. This prediction of the localization of the negligible elements permits calculation of fewer contributions and storage of only the significant terms. Secondly, the calculation of the nonnegligible elements must not be too time consuming. Finally, the computation of the system's solution must take advantage of the sparse structure of the impedance matrix.

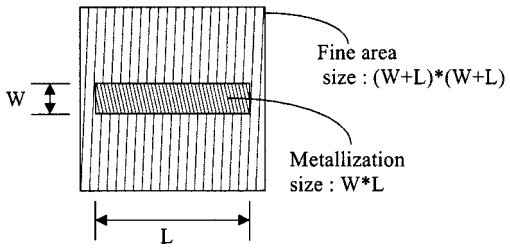


Fig. 5. Definition of the fine area.

### A. A-Priori Criterion

In (3), when the distance between the observer point $\vec{r}$ and the source point $\vec{r}'$ is "sufficient," Green's functions vary very slowly and can be represented by low-order polynomial functions. When the basis or the testing function is a wavelet, it has numerous vanishing moments. As a consequence, when these two properties are satisfied simultaneously, integrals involved in (3) become very small and the resultant matrix term can be neglected. In this section, a heuristic criterion is proposed to quantify what a "sufficient" distance should be.

Fig. 5 presents an area associated to a 1-D metallization called the "fine area." The criterion used can be stated as follows: *If the fine areas of two metallizations do not overlap, a coarse approximation is made. A coarse approximation means that when calculating interactions between the two metallizations, only the matrix terms involving two scaling functions are taken into account*. The ones that involve at least one wavelet are considered to be equal to zero. The dimensions of the fine area have been optimized experimentally and the calculation gives good results in all tested cases.

### B. Change of Basis

When two metallizations are not far away from each other or when the self interaction of a metallization is considered, the coarse approximation is not possible. In these cases, we have to evaluate more terms when calculating the interaction between these two metallizations. In particular, interactions involving wavelets are not necessarily negligible. A simple technique to compute these interactions efficiently is proposed.

The corresponding sub-matrix is first computed with rooftop basis at a fine resolution level ($s = s_u + 1$). This first step simply consists in calculating a conventional MoM sub-matrix. Through a simple change of basis, on expansion and weighting functions, the sub-matrix in the wavelet basis ($s = 2, \ldots, s_u - 1, s_u$) is then easily obtained. This change of basis is performed on columns (basis functions) and rows (testing functions) of the sub-matrix. Obviously, because of the matrix transform procedure, this technique will be more time consuming than the classical rooftop MoM, but one must remember that the transform is only applied for "local" interactions, when metallizations are close to each other. Nevertheless, the transformation time is generally negligible compared to the filling time.

Afterwards, a thresholding procedure is applied on the obtained sub-matrix. Indeed, some of the elements, even in self-interaction sub-matrices, are small enough to be neglected. In practice, elements whose modulus, normalized to the modulus of the larger element of the sub-matrix, is smaller than $10^{-5}$ are set to zero.

Another way to compute the sub-matrix would be to calculate directly all elements in the wavelet basis. However, this technique has not been chosen because it largely increases the CPU time, as can be seen in Table I. This table presents the average CPU time for the computation of a single matrix element. These results are obtained with the calculation of a simple microstrip line on an HP9000 series 160 computer. On the contrary, the change of basis only represents 2% more time in the computation of one element matrix.

Thus, for local interactions, a change of basis associated to a thresholding procedure is used. For sub-matrices involving distant metallizations, a coarse approximation is applied. The resulting MRMoM impedance matrix is then a sparse one. To benefit from this property of the linear system, a sparse solver associated to a sparse storage of the impedance matrix is chosen.

Two families of matrix solvers exist: direct and iterative. For sparse systems, iterative solvers are commonly preferred because the matrix is not modified during the inversion and it maintains its sparse behavior. Unfortunately, these solvers do not necessarily converge and the convergence rate depends on the condition number of the treated system. Thus, the direct sparse solver UMFPACK2.2[1] has been chosen.

## V. Numerical Results

In order to evaluate the real capabilities of the MRMoM, linear arrays of EMC dipoles of different size have been analyzed. These structures easily permit the study of the performance as a function of the problem size. The calculation of an EMC dipole generates a small linear system of size 50 (17 cells on the dipole and 33 cells on the feeding line) so that an array of $N$ dipoles generates a linear system of $N \times 50$ unknowns. Fig. 6 presents the studied structures made of dipoles disposed along an axis with a constant spacing of 10 mm. These elementary antennas are fed independently, thus an array of $N$ dipoles constitutes an $N$-port structure.

### A. Elementary EMC Dipole

The elementary EMC dipole is calculated with the conventional MoM, the MRMoM with compression, and the MRMoM without compression. The MRMoM is calculated through the change of basis technique because all metallization interactions are "local" and the coarse approximation is not possible. The compression rate is defined as follows:

$$R(\%) = \frac{\mathrm{NbZero}}{n^2} \times 100 \tag{9}$$

where $\mathrm{NbZero}$ is the number of elements set to zero in the compressed matrix and $n$ is the size of the linear system. In the case of the calculation of the EMC dipole, a compression rate of 50% is achieved by simply applying the thresholding scheme. As is

[1]T. A. Davis and I. S. Duff, UMFPACK version 2.2: Unsymmetric-pattern multifrontal package, 1997. [Online]. Available: ftp://ftp.cis.ufl.edu/pub/umfpack/

TABLE I
COMPARISON OF CPU TIME PER MATRIX ELEMENT FOR THE CALCULATION OF A MICROSTRIP LINE

| | Size of the linear system: 33<br>Line length: 32 mm, width: 2.2 mm (50Ω)<br>Substrate: εr = 2.55, H = 0.8mm | | |
|---|---|---|---|
| | Conventional MoM | Wavelet, computation with change of basis | Wavelet, direct computation |
| CPU time (s) | 1.41 E-03 | 1.44 E-03 | 8.95 E-03 |
| Normalized CPU time | 1 | 1.02 | 6.35 |

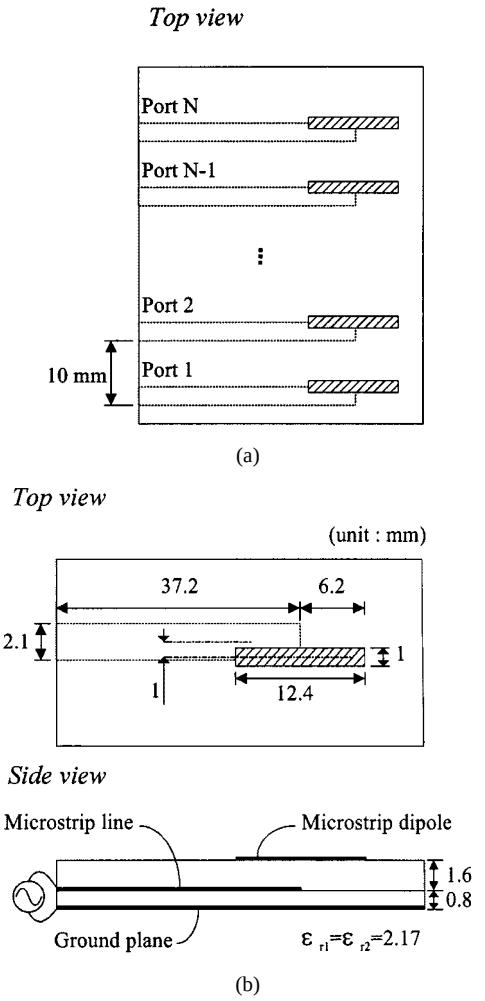


Fig. 6. (a) Array of EMC dipoles. (b) Elementary EMC dipole.

shown in Fig. 7(b), this compression does not affect the calculated input impedance. In the conventional MoM used here, the current density is expanded on a rooftop basis and pulses are used as testing functions. It is not strictly equivalent to the MRMoM that uses a quasi- Galerkin scheme, as explained previously. Nevertheless, both computations are in good agreement with experimental results. Fig. 7(a) shows a grayscale plot obtained by taking the logarithm of the elements of the compressed MRMoM impedance matrix. This clearly demonstrates that the nonnegligible elements are located on or near the diagonal or the secondary diagonals, which correspond to self-interactions or near-functions interactions.

### *B. Coupling Between Two Dipoles*

Fig. 8 shows results obtained from the study of the coupling effects between two EMC dipoles. The entire structure is first simulated using the MRMoM without neglecting elements of the impedance matrix; this calculation is called the "fine" one. In the second calculation, the coarse approach is used. Practically, in that case, it means all the terms involving wavelets are set to zero in the sub-matrix corresponding to the interaction between the two antennas.

Fig. 8(b) depicts the input impedance of the first dipole versus the normalized distance $d$. The input impedance is calculated at the frequency of 8.3 GHz, which corresponds to the resonant frequency of the dipole. First, it is noted that the coarse approximated solution is very close to the fine one. The maximum margin between the two curves, even for small distances, is about 2 dB, which means that the coarse representation of the current reasonably models coupling between metallizations. Secondly, the two results converge for distances larger than $0.5\lambda_0$. Beyond this value, the coarse approximation gives exactly the same results as the fine calculation. These results show that the criterion proposed in Section IV-A is suitable. In this case, the criterion would correspond to a normalized distance of one.

### *C. Linear Arrays*

Fig. 9 depicts the sparsity achieved when calculating the linear arrays with the MRMoM. The compression is obtained by applying the rules defined in Section IV. For an array of ten dipoles, or a system of 500 unknowns, the compression rate is already 91% and grows quickly, reaching 98% in the case of the array of 200 elements.

This sparsity permits an important reduction of the CPU time. In addition to this, the memory storage is also reduced and this reduction allows calculation of larger structures with the MRMoM than with the conventional MoM. Indeed, with the MRMoM approach, we never compute and store a dense matrix, the impedance matrix is directly stored in the sparse format. With this technique, we are able to go further than the memory limits of the computer. Here, with the available memory, it is not possible to store complex matrices larger than $5600 \times 5600$.

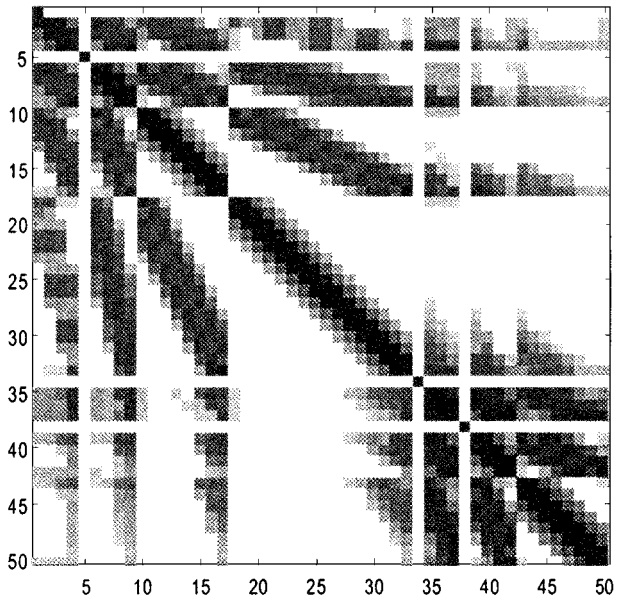


(a)

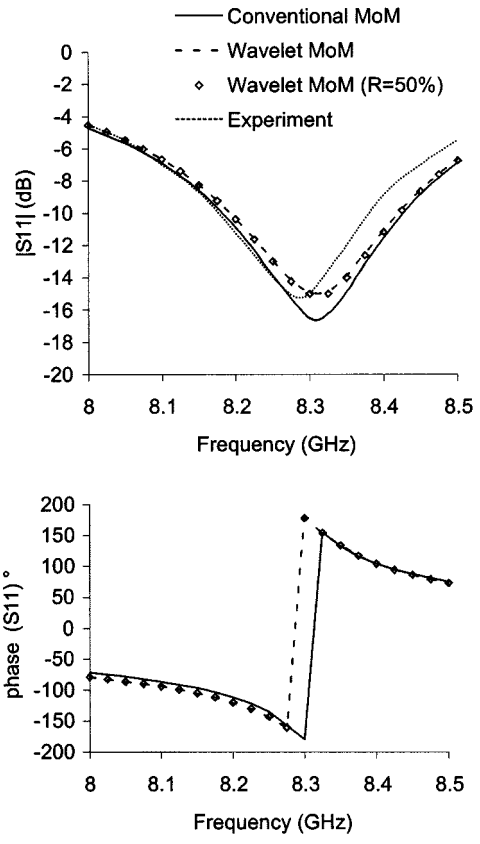


(b)

Fig. 7. Calculation results of the elementary EMC dipole.

This size corresponds to an array of 110 dipoles. In the case of the MRMoM, thanks to the achieved sparsity, we are able to compute an array of 200 dipoles. Therefore, in Fig. 10, all CPU time charts stop at arrays of 100 dipoles for the conventional MoM, while results obtained for arrays of 200 dipoles are presented in the case of the MRMoM.

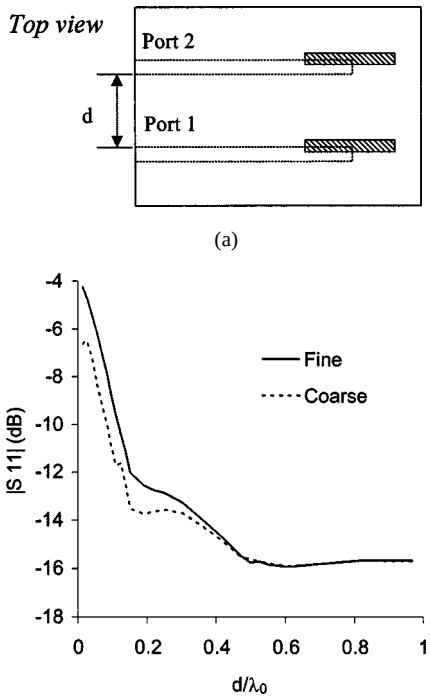


(a)




(b)

Fig. 8. Reflection coefficient as a function of the coupling.

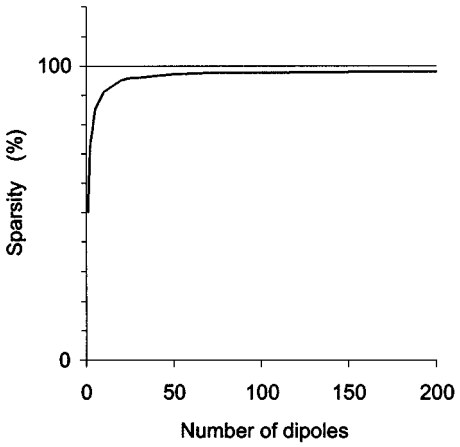


Fig. 9. Achieved matrix sparsity.

Fig. 10(a) and (b) depicts the filling time and inversion time as a function of the number of calculated dipoles. For arrays with more than 25 dipoles, the filling time is shorter in the case of the MRMoM. In the case of a 100-dipole array, the filling time is divided by a factor of four. The reduction of the inversion time is much more spectacular. In the case of the 100-element array, the matrix inversion time is divided by a factor of 13. It should be observed that, for the calculation of the solution of the conventional MoM, a direct solver is also used. This reduction is possible thanks to the achieved compression rate of 97.5%. In the case of the 200-dipole array, the calculation of the solution of the linear system of 10 000 unknowns takes only 20 min ($R = 98\%$).

In Fig. 10(c) and (d), the total calculation time as well as the total required memory are depicted as a function of the array's size. The calculation of the 100–element array is ten

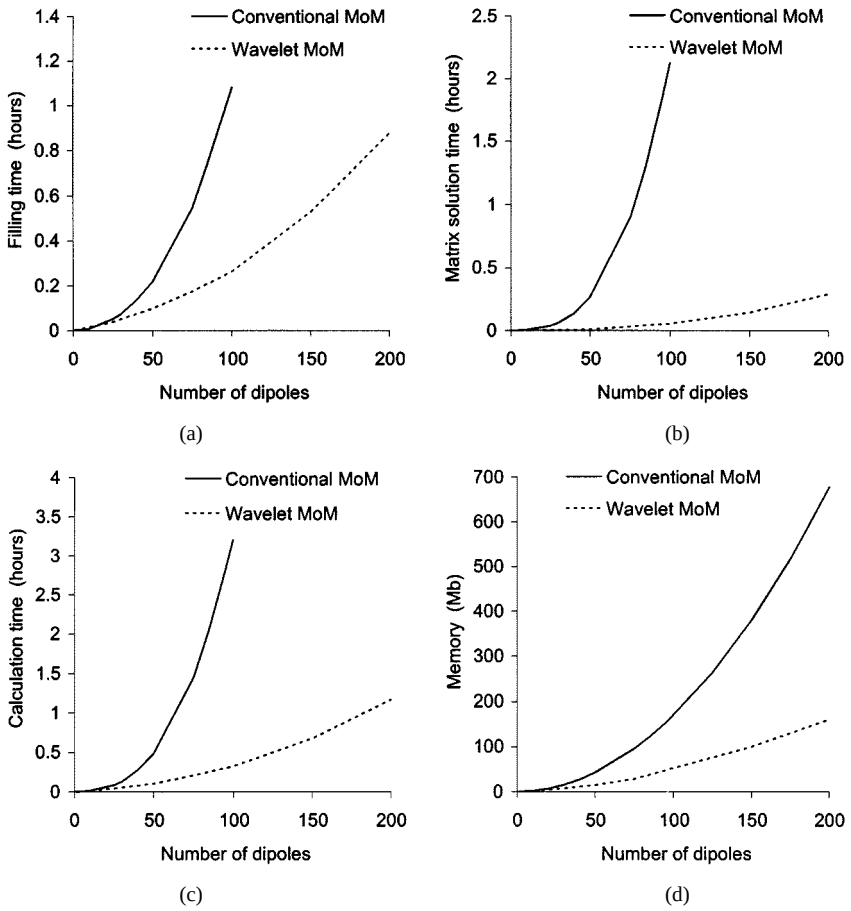


Fig. 10. Performances of the approach versus the size of the problem.

times longer and requires three times more memory with the conventional MoM than with the MRMoM. In the limiting case of 200 dipoles, the MRMoM requires 160 Mb, while the dense matrix would have needed 700 Mb to stored. These two curves demonstrate the real advantages of the MRMoM to study such structures.

Fig. 11 offers results that compare the conventional MoM and MRMoM. The required memory is plotted on a log scale. Since memory used in classical MoM has a $O(N^2)$ behavior, we can determine that for the MRMoM, the required memory has a $O(N^{3/2})$ behavior.

Fig. 12 shows the calculated radiation patterns of a ten-dipole antenna. In the two diagrams, the direct component in the $H$-plane is depicted. In Fig. 12(a), all elements are fed, while in Fig. 12(b), only the fifth element is fed and the other ports are matched. The patterns in Fig. 12(b) are called the active radiation patterns of the fifth element of the array. The radiation pattern of the single dipole has been added in order to evaluate the effects of the array on the radiation pattern of an element. This shows that the radiation pattern of a dipole in an array is less directive than the radiation pattern of an isolated dipole. In the two diagrams, results of the conventional MoM and MRMoM agree well.

## VI. Conclusion and Discussion

In this paper, a complete MRMoM analysis of 1-D structures using matched terminations has been presented. To this end, a new formulation of the MoM matched load model is proposed. Calculation rules are also given in order to optimize the algorithm and to take advantage of the wavelet scheme. The implemented algorithm has been shown to be very efficient for the simulation of linear arrays of EMC dipoles compared to conventional MoM. The calculation time is reduced by a factor of 13, while the required memory is divided by three for the calculation of a 100-dipole array. The presented technique allows the calculation of larger structures for a particular computer memory size than with the conventional MoM.

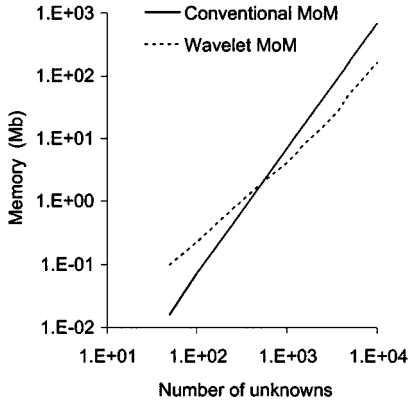


Fig. 11. Required memory versus the number of unknowns (log scale).

There is another way to use wavelets in the MoM in electromagnetic problems. As in [5], the DWT can be applied on the en-

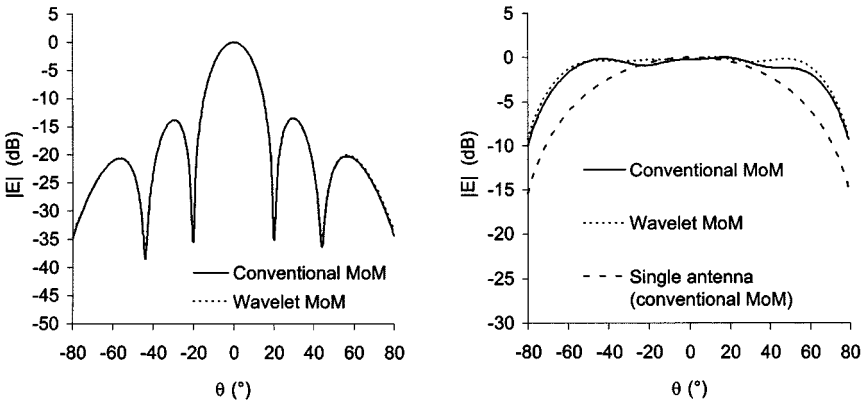


Fig. 12. Radiated fields of a ten dipole array.

tire impedance matrix calculated through a conventional MoM. In this technique, basis and testing functions do not matter, and sophisticated wavelet bases can be used even in a simple conventional MoM. In [5], Daubechies orthogonal wavelets and biorthogonal spline wavelets are used in the calculation of linear arrays of rectangular patches. The two-dimensional nature of this elementary antenna constitutes the main difference with the structures presented in this paper. In [5], the application of the DWT allows the best case to reduce the computation time by a factor of three, while the required memory is not really reduced because the entire MoM matrix must be stored before the transformation. These results are not as spectacular as results obtained with the MRMoM. With the MRMoM, the impedance matrix is directly calculated in a wavelet basis in a compressed format. By this way, the transformation time is avoided and the filling time is also reduced. This partially explains the large differences existing between the performances of the two techniques. The exact comparison will be made when the MRMoM has been extended to two-dimensional structures. This extension is currently under investigation.

## REFERENCES

[1] P. Lepeltier, J. Citerne, and J. M. Floc'h, "On the EMC dipole feed line parasitic radiation," *IEEE Trans. Antennas Propagat.*, vol. 38, pp. 878–882, June 1990.

[2] Z. Xiang and Y. Lu, "An effective wavelet matrix transform approach for efficient solutions of electromagnetic integral equations," *IEEE Trans. Antennas Propagat.*, vol. 45, Aug. 1997.

[3] R. L. Wagner and W. C. Chew, "A study of wavelets for the solution of electromagnetic integral equations," *IEEE Trans. Antennas Propagat.*, vol. 43, Aug. 1995.

[4] Z. Bahrav and Y. Leviatan, "Impedance matrix compression using iteratively selected wavelet basis," *IEEE Trans. Antennas Propagat.*, vol. 46, pp. 1231–1238, Feb. 1998.

[5] R. Loison, R. Gillard, J. Citerne, and G. Piton, "Application of the wavelet transform for the fast computation of a linear array of printed antennas," in *European Microwave Conf.*, vol. 2, Amsterdam, The Netherlands, 1998, pp. 301–304.

[6] L. P. B. Katehi, "Application of wavelets to electromagnetics, Introduction to multi-resolution analysis," presented at the IEEE MTT-S Int. Microwave Symp. Workshop, San Francisco, CA, June 1996.

[7] J. C. Goswami, A. K. Chan, and C. K. Chui, "On solving first-kind integral equations using wavelets on a bounded interval," *IEEE Trans. Antennas Propagat.*, vol. 43, pp. 614–622, June 1995.

[8] G. Oberschmidt and A. F. Jacob, "Accelerated simulation of planar circuits by means of wavelets," in *European Microwave Conf.*, Amsterdam, The Netherlands, 1998, pp. 305–310.

[9] R. Gillard, J. H Corre, M. Drissi, and J. Citerne, "A general treatment of matched terminations using integral equations—Modeling and applications," *IEEE Trans. Microwave Theory Tech.*, vol. 42, pp. 2545–2553, Dec. 1994.

[10] C. K. Chui and E. Quak, "Wavelets on a bounded interval," in *Numerical Methods of Approximation Theory*, D. Braess and C. L. Schumaker, Eds. Bassel, Germany: Binkhauser Verlag, 1992, vol. 9, pp. 53–75.

[11] J. Mosig and F. Gardiol, "A dynamical radiation model for microstrip structures," *Advances Electron. Electron Phys.*, vol. 59, pp. 139–237, 1982.

**Renaud Loison** was born on January 16, 1974, in Saint Brieve, France. He received the Diplôme d'Ingénieur degree from the National Institute of Applied Sciences (INSA), Rennes, France, in 1996, and is currently working toward the Ph.D. degree at INSA.

His current research interest concerns application of wavelets in numerical methods applied to the computer-aided design (CAD) of microwave antennas.

**Raphaël Gillard** was born on June 11, 1966, in France. He received the Diplôme d'Ingénieur and Ph.D. degrees in electronics from the National Institute of Applied Sciences (INSA), Rennes, France, in 1989 and 1992, respectively.

From 1992 to 1993, he was an Engineer with the Society IPSIS, where he was involved with commercial electromagnetic simulators. In 1993, he joined the Microwave Group, INSA, as an Associate Professor. His current research interest concerns numerical methods applied to the CAD of microwave circuits and active antennas.

**Jacques Citerne** (M'98) was born on October 5, 1945, in France. He received the Doctorate degree in physics from the University of Lille, Lille, France, in 1978.

He was Head of the Circuits and Propagation Group, Microwave and Semiconductor Center, Technical University of Lille until 1981. Since 1981, he has been a Professor of electrical engineering at the National Institute of Applied Sciences (INSA), Rennes, France, where he has been responsible for the Laboratory for Telecommunication Components and Systems (LCST), which, since 1984, has been supported by the French National Center of Scientific Research (CNRS). The activities of LCST concern microwave and millimeter-wave circuits and antennas, indoor communications, spread-spectrum systems, radar, and diffraction.

**Gerard Piton** was born in 1940. He received the Engineer degree from the Grenoble Radio Polytechnic Institute (IRG64), Grenoble, France, in 1964, and the B.Sc. degree from the Grenoble University, Grenoble, France, in 1964.

He is currently involved with satellite antennas for space telecommunications in the Antenna Department, Centre National d'Etudes Spatiales (CNES), Toulouse, France. His specific interests include research and development of printed antennas.

**H. Legay**, photograph and biography not available at time of publication.